15th SIRM – European Conference on Rotordynamics,
Darmstadt, Germany, 22nd – 24th February 2023

Numerical Evaluation of Alford Forces Acting on an Axial Expander for Supercritical CO2 Application

Edoardo Gheller [1], Steven Chatterton [1], Lorenzo Cosi [2], Gabriele Girezzi [2], Alessandro De Luca [2], Paolo Pennacchi [1]

[1] Department or Mechanical Engineering, Politecnico di Milano, 20145, Milan, Italy, {edoardo.gheller, steven.chatterton, paolo.pennacchi}@polimi.it
[2] Turbomachinery & Process Solutions, Baker Hughes, 50127, Florence, Italy, {lorenzo.cosi, gabriele.girezzi, alessandro.deluca}@bakerhughes.com

Abstract

Nowadays, supercritical carbon dioxide (S-CO2) cycles are of great interest in the scientific research especially considering the energy transition that is occurring. The S-CO2 high density and relatively low viscosity make it an interesting fluid for power generation. For large heat sources, large flowrates of fluid can be obtained. Therefore, the development of axial flow expanders can allow large power generations.

In the presence of rotor eccentricities, the aerodynamic loading of free-standing blades is not constant tangentially and will promote the lateral vibration of the rotor. The dynamic phenomenon that arises is known as Thomas-Alford force. The Thomas-Alford force determines an increase of the vibration level of the machine and a higher risk of instabilities.

In this paper, a preliminary investigation of a S-CO2 axial expander stage is performed. Different correlations proposed in the literature are adopted to estimate the magnitude of the Thomas-Alford force. A mono-dimensional code and a simplified computational fluid dynamics (CFD) model are adopted to obtain the parameters of the stage considered. In this preliminary investigation, only free-standing blades are considered.

The results obtained show a good agreement between 1D and CFD inputs required by the different correlation used. Despite this, the cross coupled stiffness calculated are widely dependent on the correlation used; then, this study can be considered as the starting point for more detailed investigations validating the correlations behavior in this environment through an unsteady CFD and/or a proper test campaign.

1 Introduction

In the energy transition and decarbonization perspective, scientific research is focusing more and more on renewable energy sources. Among the others, supercritical carbon dioxide (S-CO2) cycles are of great interest.

As reported in [1], S-CO2 cycles have a wide range of applications. They can be considered as a substitute for the water Rankine cycles in nuclear and fossil fuels power plants or they can be also applied to Waste Heat Recovery applications [9]. S-CO2 cycles can also be applied with renewable energy sources like the geothermal and the solar ones [10]. As for the fluids used in organic Rankine cycles (ORCs), S-CO2 is characterized by large density and low viscosity. The big advantage of S-CO2 is that is not flammable, not toxic, and has a much lower impact on the environment than most of the gases used for ORCs.

Typically, the power generation for Waste Heat Recovery cycles is performed by radial expanders. However, if large heat sources are available, there may be the possibility to process larger flowrates of working fluid to generate more power. For this reason, there is a great interest in developing axial expanders. However, due to the large flowrates and physical properties of the S-CO2, the blades will need to sustain large aerodynamic loading. If free-standing blades are considered, a small eccentricity of the shaft with respect to the casing would determine a non-homogenous tangential distribution of clearance. As a result, the blades will be non-homogeneously loaded. Eventually, the inhomogeneity of the load causes unsteady forces orthogonal to the defection which promotes the vibration of the shaft and increases the risk of instabilities. This phenomenon is known as Alford force in the literature. Actually, it was first investigated by Thomas [19] in 1958 for axial turbines and then by Alford [2] in

1965 for axial compressors (indeed, for turbomachinery in general). Most of the papers of Thomas were written in German, and were not popular in the United States, so the phenomenon started to be named in the English literature as “Alford force”.

As reported in [18], the model proposed by Thomas for turbines is generally accepted. In the case of an eccentricity as that shown in Figure 1, the effect of the horizontal force F_x can be modeled by means of as a cross coupled stiffness K_{xy}:

$$K_{xy} = \frac{F_x}{+Y} = \frac{T\beta}{D_p h} \tag{1}$$

where $+Y$ is the shaft deflection, T is the stage torque, D_p is the mean diameter and h is the blade height. Parameter β was introduced by Alford as the change in the thermodynamic efficiency but now is considered as an empirical factor to match computational predictions with experimental data. For turbines, generally $1 < \beta < 5$, [18].

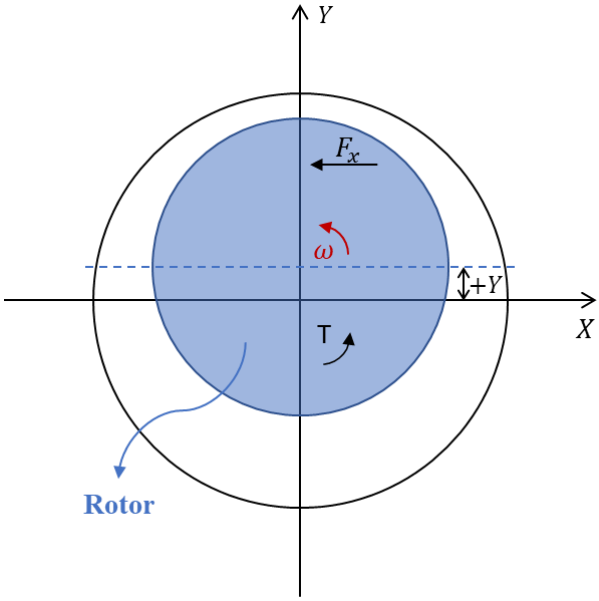

Figure 1: Schematic representation of whirling rotor.

Different models regarding axial compressors are present in the literature.

Ehrich et al. proposed the parallel compressor model, [6], where the shaft whirling is neglected and a static eccentricity is considered instead. The circumferential evolution of the clearance is considered half at minimum clearance and half at maximum clearance.

Spakovszky et al. in [17] considered the non-stationary motion of the shaft for which a complex fluid model is adopted to extract the flow quantities necessary for the evaluation of the Alford force.

Song and Cho in [14] presented a model to evaluate the rotodynamic forces in a compressor generated by non-uniform tip clearance. The model is based on the analysis presented by Song and Martinez-Sanchez in [15,16] developed for axial turbines and on the experimental campaign presented in [11] and is based on the “actuator disk” approach. The modeling of the flow in the clearance region is also necessary.

More recently, Pan et al. in [12,13] investigated with Computational Fluid Dynamics (CFD) the dynamic forces acting on an off-centered un-shrouded axial steam turbine. The authors also investigated the shape of the tip of the blade and the clearance on the dynamic forcing. In [3], the authors proposed a CFD study on the first stage of a high-pressure steam turbine focused on the effect of the shroud and labyrinth seals.

In [8], Ehrich et al. compared the results obtained with the previously mentioned models with experimental results obtained with a testbench recreating the operation of an axial compressor.

A similar phenomenon happens also in the case of shrouded blades. As reported by Alford [2], the shaft orbiting causes a tangential non-homogeneous distribution of pressure inside the seal that eventually worsen the orbiting phenomenon. Similar conclusions are reported by Ehrich et al. in [7]. More recently, CFD was applied to study the effect of dry gas seal of radial expanders for S-CO2 applications, [20,22,23]. In [21], the authors investigated the effect of the length, depth, and number of teeth on the performance of a labyrinth seal for S-CO2 applications. In [4,5], the authors presented a detailed study on the effect of shroud seals on the fluid flow of an axial S-CO2 turbine stage.

Regarding the blade aerodynamic forcing, most of the research present in the literature focused on axial compressors since they are more sensible to instabilities than turbines. However, the physical properties of S-CO2 are very different from those of the gases usually processed in axial expanders. The aerodynamic loading exerted by the S-CO2 on the blades can be significantly higher than the one exerted by steam. Therefore, it is worth to address this topic in the design of the axial turbine for S-CO2 cycles.

In this paper, a stage of an axial expander for S-CO2 is considered. The stage parameters are extracted with two approaches. At first, a simplified mono-dimensional model based on the mean line approach is applied; then, a CFD model of the blade channel is used along with the simulation of the leakage flow at the tip of the blade. In Section 2, the models used for the evaluation of the stage parameters are introduced together with the correlations adopted to evaluate the Alford force. The results obtained are reported and discussed in Sections 3 and 4 respectively. The prediction of the Alford forces is partially affected by the model selected for the evaluation of the stage parameters (1D and CFD are almost aligned) and, above all, by the correlation used. Finally, the conclusion are drawn in Section 5.

The results reported in this paper highlight the necessity to further investigate the phenomenon at least for a validation of the correlation that is more accurate for S-CO2 application. However, also more sophisticated models to extract the stage parameters will be helpful in improving the estimation of the Alford force. Another approach, in the short term and beyond a test case with the required geometric and thermodynamics conditions, could be to address this subject as a sensitivity analysis on a full rotor behavior to evaluate if the instability risk is avoided even with the most – conservative correlation that provide the worst cross – coupled stiffness.

2 Materials and Methods

2.1 Stage parameters

The investigation is focused on a stage of an axial turbine for S-CO2 applications. A simplified meridional view of the flow path is shown in Figure 2.

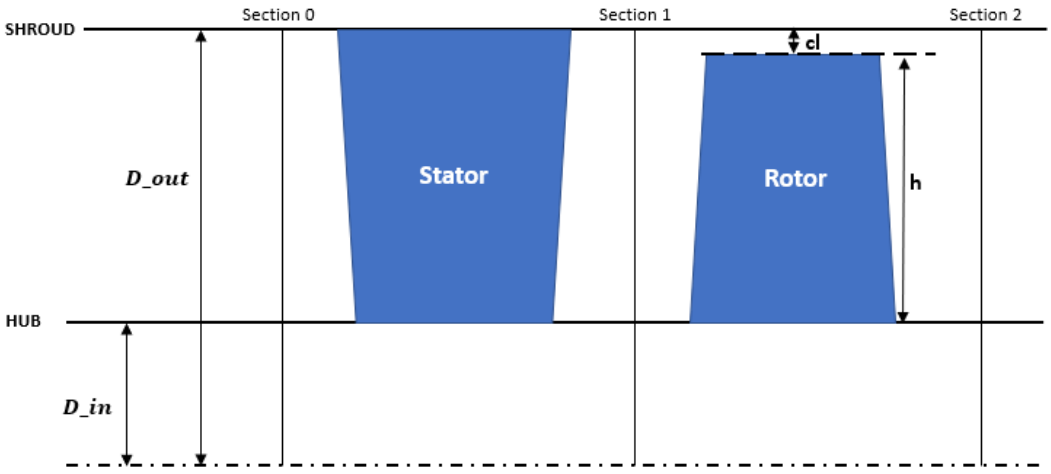

Figure 2: Stage 2D schematization.

The outer and inner diameters are respectively D_{out} and D_{in}, h is the rotor blade height and cl is the radial tip clearance between the rotor blade and the shroud casing. The mean diameter D_p is calculated as:

$$D_p = D_{in,2} + \frac{h}{2} \tag{2}$$

The rotor blade is unshrouded. The analysis is carried out at five different levels of clearance. The percent increments with respect to the nominal clearance (cl_1) are listed in Table 1.

Table 1: Dimensionless levels of rotor blade clearance considered for analysis.

cl_1	cl_2	cl_3	cl_4	cl_5
1	*1.24*	*1.42*	*1.61*	*1.79*

2.2 1D model

At first, the analysis is carried out at mean-line level. A 1D code works on a single geometric streamline, the mean-line, where it solves the velocity triangles of a turbine stage by means of loss and deviation correlations. The losses of the row are estimated together with the turn efficiency considering different loss mechanisms. Clearly, blade geometry is reduced to a short set of parameters complemented by default rules.

The total-to-total pressure ratio is considered fixed for the 5 levels of tip clearance reported in Table 1. The tip clearance is assumed uniform tangentially. The 1D model returns the estimated performance of the stage at the design point (cl_1) and at the four off-design conditions ($cl_2 - cl_5$). The outputs include the torque generated by the rotor blading which serves as input for all the models presented in the first paragraph. The information made available by the 1D code provides a measure of the efficiency penalty and of the power/torque reduction as a function of the tip clearance.

Therefore, the underlying assumption for the subsequent rotor dynamic analysis is that the outputs of those five runs are to be merged to model a unique non-uniform tangential distribution of torque. Considering the highly unsteady nature and tangential non-uniformity of the investigated phenomenon, this is of course a significant simplification to be validated by more complex modelling strategies.

Two more assumptions need to be introduced. The fluid is treated as a semi-perfect gas. The approximation on the evaluation of the thermodynamic properties with respect to a rigorous real fluid modelling is negligible considering the narrow thermodynamic space covered by the expansion of a single stage and the wide margin from the phase transition guaranteed by the highly supercritical conditions imposed by the cycle. The second assumption is on the secondary flows. Given the purpose of this assessment, neither wheel space nor shroud cavities are included in the calculation domain to avoid unnecessary complexity for the 3D CFD analysis and not to taint the evidences related to the investigated phenomenon.

2.3 CFD model

The same approach and assumptions of the 1D model are adopted for the 3D CFD analysis carried. The commercial code ANSYS CFX is selected for the analysis. For each tip clearance level, a RANS (Reynolds-averaged Navier Stokes) simulation is run.

The single-block grids (OH type) are realized in Numeca AutoGrid™ environment and are then imported in ANSYS CFX. The mesh, with more than 1.5 million elements for both stator and rotor, is built to comply with all the standard quality metrics. The clearance region above the blade tip is meshed with a number of cells in the radial direction proportional to the opening itself (increasing from cl_1 to cl_5) as the blade is of the unshrouded type. Boundary conditions and fluid modelling are the same of the 1D model setup. The selected turbulence model, common to all the cases, is the SST K-Omega, typical option for gas turbine CFD simulations. This model combines the advantages of the K-Epsilon for the free-stream region with those of the K-Omega for the resolution of the boundary layer. Therefore, it offers a good prediction of flow separation and the ability to account for the transport of the principal shear stress in adverse pressure gradient boundary layers. The turbulence model selection is not expected to significantly affect the analysis results provided that the turbulence properties are correctly initialized. A medium level of turbulence intensity is applied as a boundary condition for all the investigated cases. Furthermore, the presence of the meshed clearance (symmetric or asymmetric) region above the blade tip is not driving the turbulence model selection as SST K-Omega is expected to return accurate results in any near-wall regions, blade tip included.

In summary, the analysis setup fully adheres to the standard template adopted for CFD analysis on gas turbines.

3D CFD enables the detailed assessment of the flow field of the tip clearance. The information extracted from the simulation post processing is anyway the overall torque of the stage, as required by all the correlations evaluating Alford forces.

2.4 Correlations

The dimensionless stage torques obtained for the different clearances of the rotor blade, and used to feed the correlations, are presented in Figure 3. Dimensionless torques is obtained by normalizing the dimensional torque by the value obtained for cl_1 .

The Alford correlation has been shown in Equation (1). The cross-coupled stiffness coefficient K_{xy} is evaluated for different values of the parameter β .

In [6] the parallel compressor model is introduced. The static eccentricity Y is considered and the whirling motion is neglected. The tangential distribution of clearance is simplified as shown in Figure 4. Half the rotor has the minimum radial clearance (cl_1). The other half has the maximum radial clearance (cl_5).

In [6], Ehrich proposed to evaluate β as:

$$\beta = \frac{2(T_5 - T_1)}{(T_5 + T_1)\left[\left(\frac{cl}{h}\right)_5 - \left(\frac{cl}{h}\right)_1\right]} \tag{3}$$

where T_5 and T_1 are the stage torques for cl_5 and cl_1 respectively.

Once β is calculated, Equation (1) is applied to evaluate the Alford force.

In [17], the effect of the whirling motion is taken into consideration. However, neither the 1D model nor the CFD model can be applied to obtain the unsteady flow quantities. Therefore, a simplified approach is considered. The tangential evaluation of the aerodynamic forces is evaluated only considering an eccentric rotor. For the analysis, $100\ \mu m$ and $200\ \mu m$ peak-to-peak eccentricities are considered for the minimum and the maximum clearance values in Table 1. The tangential distribution of the torque T_θ caused by the static eccentricity is obtained with an interpolation.

Then, the tangential distribution of the force f_θ is:

$$f_\theta = \frac{T_\theta}{D_p} \tag{4}$$

The tangential evolution of f_θ for the 1D model and the CFD model are shown in Figure 5.

If synchronous *1X* vibrations are considered, the force F_x is defined as:

$$\begin{bmatrix} F_x \\ F_y \end{bmatrix} = \begin{bmatrix} 1 & 0 \\ 0 & 1 \end{bmatrix} \begin{bmatrix} \int_0^{2\pi} f_\theta \sin(\vartheta)\, d\vartheta \\ -\int_0^{2\pi} f_\theta \cos(\vartheta)\, d\vartheta \end{bmatrix} \tag{5}$$

where ϑ is the tangential coordinate.

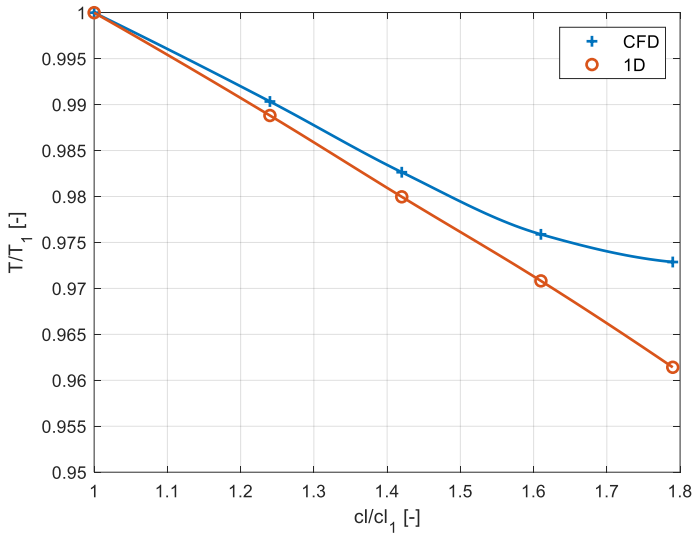

Figure 3: Torque at different levels of rotor blade clearance - 1D vs CFD.

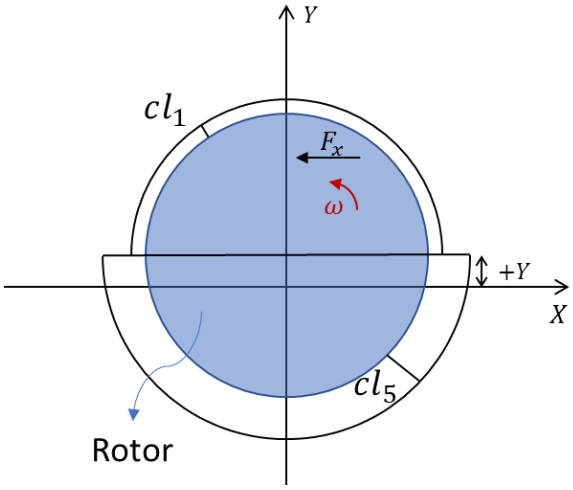

Figure 4: Schematic representation of parallel compressor model, [6].

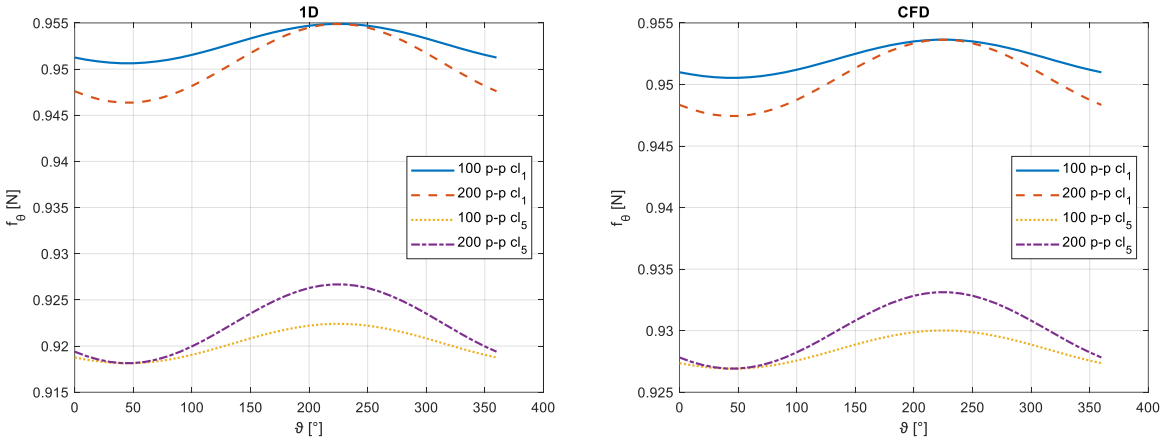

Figure 5: Tangential evolution of f_θ for *100* and *200 p-p* eccentricity for cl_1 and cl_5. (Left) 1D model, (Right) CFD model

3 Results

The results obtained with the different correlations are presented in this section. The evolution of the absolute value of K_{xy} with the radial clearance for the 1D and CFD models is shown in Figure 6. Those results are obtained by applying the Alford correlation, Equation (1), to the data shown in Figure 3 and in Table 1.

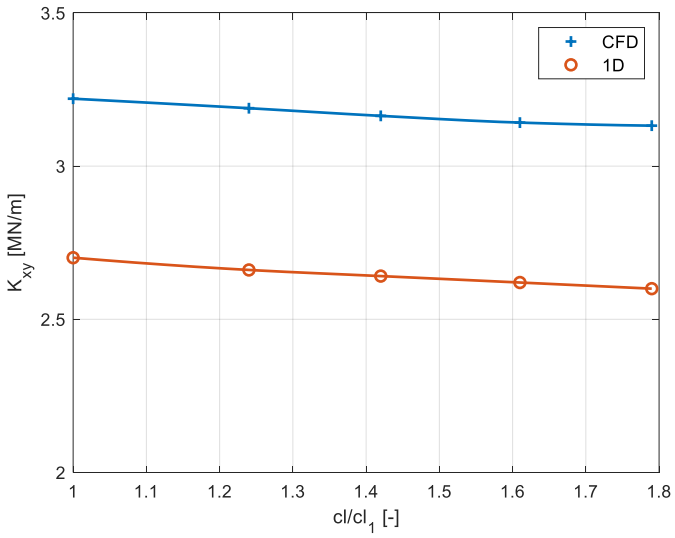

Figure 6: Evolution of K_{xy} with tip clearance considering Alford correlation for 1D and CFD model.

If β is calculated according to in Equation (3), the resulting values obtained for K_{xy} by applying Equation (1) are listed in Table 2. Both the 1D and CFD models are considered. Results reported by Figure 6 and Table 2 highlight that the cross-coupled stiffness is approximately constant over the evaluated clearance domain while it shows a large variability based on the correlation used for the Alford force estimation. Therefore, from now on, the results are presented as average values covering the whole tip clearance span.

Table 2: Results for Ehrich correlation for 1D and CFD model.

Model	$\boldsymbol{\beta}$	$\boldsymbol{K_{xy}\,[MN/m]}$
1D	*-2.15*	*-5.78*
CFD	*-1.50*	*-4.77*

Equation (5) is applied to obtain F_x in the case of Spakovszky correlation. Then Equation (1) is applied to calculate K_{xy}. In this case, the static eccentricity considered is $+Y = 50\mu m$ for the $100\mu m$ peak-to-peak case and $+Y = 100\mu m$ for the $200\mu m$ peak-to-peak. The results obtained for the 1D model and the CFD model are listed in Table 3. Since these results are not affected by the clearance and the static eccentricity, only the results for cl_1 and $+Y = 50\mu m$ are reported; it is strictly connected to the definition reported in Equation (5) where a double force value variation due to a double amplitude is divided by a double eccentricity.

Table 3: Results for Spakovszky correlation for 1D and CFD model.

Model	**Clearance level**	$\boldsymbol{+Y\,[\mu m]}$	$\boldsymbol{K_{xy}\,[MN/m]}$
1D	*1*	*50*	*-0.44*
CFD	*1*	*50*	*-0.38*

4 Discussion

Considering the results of application of the Alford correlation, reported in Figure 6, lower cross-coupled stiffness and then aerodynamic forces are obtained if the 1D model is considered instead of the CFD one. With this difference on the inputs required for the correlation, the difference between the 1D and CFD results is around -15%. In addition, directly connected to the slope of trending lines of Figure 3, the impact on torque of radial clearance variation of the rotor blade is larger for 1D than CFD model, respectively 4% for the 1D model and 3% for the CFD model.

According to the frame of reference indicated in Figure 1, a negative value of the cross-coupled stiffness K_{xy} indicates the promotion of forward whirl, typical for turbines, [18]. The torque positive direction selected in this paper is the opposite than the one indicated by Alford, [2]. Therefore, the values of K_{xy} shown in Figure 6 are negative ad forward whirl is predicted with the Alford correlation. When the Ehrich correlation is applied to both the 1D and CFD model negative values for β are obtained, see Table 2. Therefore, negative values are obtained for K_{xy} predicting a forward whirl phenomenon. Since the Ehrich correlation is more connected to the torque variation with clearance, it is quite straightforward that the larger cross-coupled stiffness is obtained for 1D model that is characterized by a higher trending line slope, see Figure 3. Moreover, the simplified 1D model overestimates of $+21\%$ the value of K_{xy} with respect to the CFD prediction.

The results obtained with the Spakovszky correlation are listed in Table 3. Also in this case a forward whirl is predicted. The discussion provided on the results obtained with the Ehrich correlation is applicable also in this case. However, the results obtained with the Spakovszky correlation are one order of magnitude lower than the results obtained with the Ehrich correlation. As a matter of fact, both the 1D and CFD results are much lower, in absolute value, than the ones obtained with the Alford and Ehrich correlations. The hypotheses of stationary condition and the interpolation of the torque tangential evolution are too strict, and the results obtained could lose significance. On the other hand, it could be that this last correlation, more connected to the aerodynamic behaviour of the analysed stage, provides results closer to the real phenomenon. However, a more detailed investigation is required to reduce the uncertainty for this application.

As summary, the results reported in this paper are an initial evaluation of the Alford effect for a S-CO2 application. Different behaviours are obtained considering the different correlations. Different results are obtained with the application of the 1D and CFD models. However, the major effect on the value of the cross-coupled stiffness K_{xy} is related to the choice of the correlation. From a quantitative point of view, the Ehrich correlation provides values higher than the ones obtained with the Alford correlation of 110% for the 1D model and 48% for the CFD model. Similarly, the Spakovszky correlation provides, in general, values an order of magnitude lower if compared both with the Ehrich and Alford correlations. As highlighted by the results shown in this paper, both the 1D and CFD model give comparable results. Therefore, the simplified 1D approach can be used for the investigation at this stage of the analysis since the flow path modelling is not as impacting as the choice of the correlation. A more detailed investigation of the effect of the Alford force on this S-CO2 application is required.

5 Conclusions

In this paper, the Alford effect in an axial turbine stage for S-CO2 application is investigated. The Alford effect is introduced using the different empirical correlations already published in the literature.

The parameters characterizing the stage are obtained with a 1D mean line model and a CFD model. The Alford, Ehrich, and Spakovszky correlations are selected, considering the data available for the 1D and CFD models considered and their results on the estimation of K_{xy} are shown. All three models agree in the prediction of forward whirl excitation, a typical phenomenon for axial turbines. Nonetheless, a deeper investigation is required to fully comprehend the phenomenon of the Alford force.

Focusing on the numerical models adapted, the uncertainty introduced in the analysis by using the 1D or the CFD model is an order of magnitude lower than the uncertainty in the final value of the cross-coupled stiffness obtained with the different correlations. Therefore, reliable results can be obtained applying the 1D model, reducing the complexity and computational cost required by analysis based on CFD. It is understood that the fairly good agreement between 1D and CFD results can be leveraged as far as overall performance parameters and/or section averaged quantities are to be provided to Alford effect correlations. Therefore, 1D data provide consistent feedback when dealing with the conceptual and the preliminary design phases of new products. The use of CFD data is recommended for detailed analyses to be executed once the flow path design is mature, thus enabling the designer to evaluate local flow conditions and to estimate the impact related to the introduction of complex 3D geometrical features.

In general, the correlations considered agree that the cross-coupled stiffness estimated for the considered stage is of the order of $10^6\ N/m$. This value is generally common for a whole turbine and not for a single stage as in this case; this result is an additional confirmation of the huge impact of the S-CO2 density and of the need to properly address this phenomenon on the development of an axial turbine for S-CO2 power generation.

Future works are necessary to better understand the phenomenon of the Alford force on the S-CO2 applications at least for a validation of the correlation that is more accurate for them. To get a proper validation, the only worthwhile way is a specific test bench even simplified but capable to reproduce the phenomenon. However, also more sophisticated models to extract the stage parameters will be helpful in improving the estimation of the Alford force. In the short term, without developing an experimental test rig that reproduces the geometrical and thermodynamic conditions, a sensitivity analysis can be performed on the whole rotor structure. The instability

risk should be assessed considering the different values of the cross-coupled stiffness obtained with the different correlations to establish how harmful the Alford force can be for this application.

References

[1] Ahn, Y., Bae, S.J., Kim, M., Cho, S.K., Baik, S., Lee, J.I., et al. (2015) Review of supercritical CO2 power cycle technology and current status of research and development. *Nuclear Engineering and Technology*. 47 (6), 647–661.

[2] Alford, J. (1965) Protecting Turbomachinery From Self-Excited Rotor Whirl. *Journal of Engineering for Gas Turbines and Power*. 333–342.

[3] Cao, L.H., Wang, J.X., Li, P., Hu, P.F., and Li, Y. (2017) Numerical Analysis on Steam Exciting Force Caused by Rotor Eccentricity. *Shock and Vibration*.

[4] Du, Q. and Zhang, D. (2020) Numerical Investigation on Flow Characteristics and Aerodynamic Performance of a 1.5-Stage SCO2 Axial-Inflow Turbine with Labyrinth Seals. *Applied Sciences (Switzerland)*. 10 (1).

[5] Du, Q., Zhang, L., Zhang, D., and Xie, Y. (2020) Numerical investigation on flow characteristics and aerodynamic performance of shroud seal in a supercritical CO2 axial-flow turbine. *Applied Thermal Engineering*. 169.

[6] Ehrich, F. (1993) Rotor whirl forces induced by the tip clearance effect in axial flow compressors. *Journal of Vibration and Acoustics, Transactions of the ASME*. 115 (4), 509–515.

[7] Ehrich, F. (1968) Aeroelastic instability in labyrinth seals. *Journal of Engineering for Gas Turbines and Power*. 90 (4), 369–374.

[8] Ehrich, F.F., Spakovszky, Z.S., Martinez-Sanchez, M., Song, S.J., Wisler, D.C., Storace, A.F., et al. (2000) Unsteady Flow and Whirl-Inducing Forces in Axial-Flow Compressors: Part II—Analysis. *Journal of Turbomachinery*. 123 (3), 446–452.

[9] Kim, Y.M., Sohn, J.L., and Yoon, E.S. (2017) Supercritical CO2 Rankine cycles for waste heat recovery from gas turbine. *Energy*. 118 893–905.

[10] Li, M.J., Zhu, H.H., Guo, J.Q., Wang, K., and Tao, W.Q. (2017) The development technology and applications of supercritical CO2 power cycle in nuclear energy, solar energy and other energy industries. *Applied Thermal Engineering*. 126 255–275.

[11] Martinez-Sanchez, M., Jaroux, B., Song, S.J., and Yoo, S. (1995) Measurement of turbine blade-tip rotordynamic excitation forces. *Journal of Turbomachinery*. 117 (3), 384–392.

[12] Pan, Y., Yuan, Q., Huang, G., Gu, J., Li, P., and Zhu, G. (2020) Numerical investigations on the blade tip clearance excitation forces in an unshrouded turbine. *Applied Sciences (Switzerland)*. 10 (4).

[13] Pan, Y., Yuan, Q., Huang, G., Zhu, G., and Li, P. (2020) Numerical analysis of the aerodynamic performance and excitation forces in a transonic turbine cascade with flat-tip and squealer-tip blades. *Proceedings of the Institution of Mechanical Engineers, Part C: Journal of Mechanical Engineering Science*. 234 (22), 4377–4389.

[14] Song, S.J. and Cho, S.H. (2000) Nonuniform flow in a compressor due to asymmetric tip clearance. *Journal of Turbomachinery*. 122 (4), 751–760.

[15] Song, S.J. and Martinez-Sanchez, M. (1996) Rotordynamic forces due to turbine tip leakage - Part I: Blade scale effects. in: ASME 1996 International Gas Turbine and Aeroengine Congress and Exhibition, GT 1996.

[16] Song, S.J. and Martinez-Sanchez, M. (1996) Rotordynamic forces due to turbine tip leakage - Part II: Radius scale effects and experimental verification. in: ASME 1996 International Gas Turbine and Aeroengine Congress and Exhibition, GT 1996.

[17] Spakovszky, Z.S. (2000) Analysis of aerodynamically induced whirling forces in axial flow compressors. in: Proceedings of the ASME Turbo Expo, .

[18] Storace, A.F., Wisler, D.C., Shin, H.-W., Beacher, B.F., Ehrich, F.F., Spakovszky, Z.S., et al. (2000) Unsteady Flow and Whirl-Inducing Forces in Axial-Flow Compressors: Part I—Experiment. *Journal of Turbomachinery*. 123 (3), 433–445.

[19] Thomas H.J. (1958) Instabile Einenschwingungen von Turbinenläufern angefacht durch die Spaltströmungen Stopfbuschen und Beschauflungen. *Bull. de l'A.I.M*. 71 (11/12), 1039–1063.

[20] Yang, J., Zhao, F., Zhang, M., Liu, Y., and Wang, X. (2021) Numerical analysis of labyrinth seal performance for the impeller backface cavity of a supercritical CO2 radial inflow turbine. *CMES - Computer Modeling in Engineering and Sciences*. 126 (3), 935–953.

[21] Yuan, H., Pidaparti, S., Wolf, M., Edlebeck, J., and Anderson, M. (2015) Numerical modeling of supercritical carbon dioxide flow in see-through labyrinth seals. *Nuclear Engineering and Design*. 293 436–446.

[22] Zhu, D. and Bai, S. (2021) Ultra-high-speed TEHL characteristics of T-groove face seal under supercritical CO2 condition. *Industrial Lubrication and Tribology*. 73 (3), 523–530.
[23] Zhu, D. and Bai, S. (2021) Thermoelastohydrodynamic characteristics of supercritical CO2 spiral groove face seals. *Industrial Lubrication and Tribology*. 73 (1), 153–162.